

*The impact of spin up and resolution on the representation of a clear convective boundary layer over London in order 100m grid-length versions of the Met Office Unified Model*

Article

Accepted Version

Lean, Humphrey W., Barlow, Janet F. and Halios, Christos H. (2019) The impact of spin up and resolution on the representation of a clear convective boundary layer over London in order 100m grid-length versions of the Met Office Unified Model. *Quarterly Journal of the Royal Meteorological Society*, 145 (721). pp. 1674-1689. ISSN 1477-870X doi: <https://doi.org/10.1002/qj.3519> Available at <https://centaur.reading.ac.uk/83252/>

It is advisable to refer to the publisher's version if you intend to cite from the work. See [Guidance on citing](#).

To link to this article DOI: <http://dx.doi.org/10.1002/qj.3519>

Publisher: Royal Meteorological Society

All outputs in CentAUR are protected by Intellectual Property Rights law, including copyright law. Copyright and IPR is retained by the creators or other copyright holders. Terms and conditions for use of this material are defined in

the [End User Agreement](#).

[www.reading.ac.uk/centaur](http://www.reading.ac.uk/centaur)

## **CentAUR**

Central Archive at the University of Reading

Reading's research outputs online

# **The impact of spin up and resolution on the representation of a clear convective boundary layer over London in order 100m grid-length versions of the Met Office Unified Model.**

H.W.Lean<sup>1</sup>, J.F.Barlow<sup>2</sup>, C.H.Halios<sup>2</sup>

1. MetOffice@Reading, Meteorology Building, University of Reading, Reading RG6 6BB
2. Department of Meteorology, University of Reading, Reading RG6 6BB

\*Corresponding author: *Humphrey.lean@metoffice.gov.uk*

Key words: Convective boundary layer, turbulence, mixing height, urban meteorology, turbulence grey zone, spin up effects, spectral analysis, Doppler lidar.

## 1 **Abstract**

2 With a number of operational centres looking forward to the possibilities of “city scale” NWP  
3 and climate modelling it is important to understand the behaviour of order 100m models over  
4 cities. A key issue is how to handle the representation of partially resolved turbulence in these  
5 models. In this paper we compare the representation of a clear convective boundary layer  
6 case in London in 100m and 50m grid-length versions of the Unified Model (MetUM) with  
7 observations. Comparison of Doppler lidar observations of the vertical velocity shows that  
8 convective overturning in the boundary layer is broadly well represented in terms of its depth  
9 and magnitude. The role of model resolution was investigated by comparing a 50m grid-  
10 length model with the 100m one. It is found that, although going to 50m grid-length does not  
11 greatly change many of the bulk properties (mixing height, heat flux profiles, etc.) the spatial  
12 structure of the overturning is significantly different. This is confirmed with spectral analysis  
13 which shows that the 50m model resolves significantly more of the energetic eddies, and a  
14 length scale analysis that shows the 50m and 100m models produce convective structures 2-3  
15 times larger than observed. We conclude that, for the MetUM, model grid-lengths of order  
16 100m may well be sufficient for predicting many bulk and statistical properties of convective  
17 boundary layers however the details of the spatial structures around convective overturning in  
18 these situations are likely to be still under-resolved. Spin up artefacts emanating from the  
19 inflow boundary of the model are investigated by comparing with a smaller 100m grid-length  
20 domain which is more dominated by such effects. These manifest themselves as along wind  
21 boundary layer rolls which produce a less realistic comparison with the lidar observations. A  
22 stability analysis is presented in order to better understand the formation of these rolls.

## 23 **1. Introduction**

24 Operational regional NWP has been transformed in the last ten years by the introduction of  
25 km scale “convection permitting models” (Clark et al., 2016). More recently these models  
26 have been used for climate simulations (Kendon et al., 2014). These models have proved  
27 particularly useful because of their improved representation of convection (Prein et al., 2015,  
28 Clark et al., 2016). Higher resolution has meant that larger cities and their impact on the  
29 atmosphere can now be at least crudely represented within NWP and climate models (e.g.  
30 Holt and Pullen, 2007, Miao et al., 2009, Bohnenstengel et al., 2011, Chen et al., 2011)  
31 although smaller cities and neighbourhood scale features within larger ones cannot. With the  
32 continuing advances in available computer power a number of operational centres are now  
33 carrying out research into a new generation of city scale models at turbulence permitting  
34 (O(100m)) scales (Leroyer et al., 2014, Ronda et al., 2017). The motivation for this is to  
35 improve small scale forecasts of hazards (urban heat, flooding, poor air quality) on both  
36 weather and climate timescales. In contrast to the current generation of km scale models these  
37 models would provide the potential to represent features on neighbourhood scales (e.g. parks,  
38 rivers etc) and their effect on the local meteorology.

39 There are two aspects to the problem of developing urban models at these scales. Firstly there  
40 is the problem of the best way to represent the urban surface (Best et al., 2015). Barlow et al.  
41 (2017) identified the main problems as being heterogeneity on many scales, and  
42 anthropogenic effects. Models at 100m scales will have to operate between the traditional  
43 convection permitting NWP regime where there are many buildings per grid-box and the very  
44 high resolution regime of LES modelling of individual buildings and streets (the so called  
45 “building grey zone”). There is also the need to treat the vertical extent of buildings in high  
46 rise cities and small groups of tall buildings. It will also be very important to introduce

47 realistic anthropogenic fluxes of heat and moisture. This can either be done through  
48 interfacing the model to datasets of anthropogenic emissions (Allen et al., 2011) or by  
49 incorporating parameterisations of building and transport emissions (e.g. Bohnenstengel et  
50 al., 2014).

51 The second part of the problem is the behaviour of the atmospheric model itself in the  
52 turbulence permitting regime.  $O(100\text{m})$  grid-length models will operate in the boundary layer  
53 “grey zone” or “terra incognita” (Wyngaard, 2004, Honnert et al., 2011). There has been a  
54 good deal of work within the Met Office on pushing the Unified Model (MetUM) to sub  
55 kilometre scales. A 100m grid-length MetUM configuration was used to simulate cold pools  
56 in valleys which would have been too small to resolve with the operational 1.5km model  
57 (Vosper et al., 2013) giving good agreement with observations. Models with several grid-  
58 lengths between 1km and 100m were compared to aircraft observations of stratocumulus  
59 (Boutle et al., 2014). Hanley et al., 2016) investigated explicit representation of tornadoes on  
60 the US Great Plains with a 100m model. Similar UM configurations were also used to  
61 investigate the resolution dependence of the representation of deep convection over the UK  
62 as part of the DYMECS project (Stein et al., 2015, Hanley et al., 2015). Elsewhere in the  
63 community there have been a number of experiments with sub-km NWP models of cities  
64 (Ronda et al., 2017, Leroyer et al., 2014).

65 This paper addresses this second part of the problem in the case of clear convective boundary  
66 layers. In the current work, the model is run with the same urban surface scheme (Best,  
67 2005) as the 1.5km operational model used at the time of the case being studied. Even though  
68 the representation of the urban surface will be imperfect, we would still expect benefits from  
69 resolving relatively short range variations in the surface properties – in particular the surface  
70 type and orography. The former allows study of changes of boundary layer properties as air  
71 flows over the city. This approach has been highlighted by Ronda et al. (2017) who used

72 detailed surface input data in a 100m grid-length WRF configuration to produce  
73 neighbourhood scale forecasts during a summer period in Amsterdam.

74 Of particular relevance to this paper is the DYMECS work mentioned above which  
75 concluded that MetUM configurations with grid-lengths smaller than 1km do better for deep  
76 convection than the operational 1.5km model, (better convection lifecycle, distribution of  
77 rainrates, cell sizes etc) but there are still issues. In particular, if the model is run with a 3D  
78 Smagorinsky (Smagorinsky, 1963) subgrid mixing scheme with the usual LES value of  
79 mixing length of 0.2 of the grid-length, convective updrafts and cells tend to become too  
80 narrow at the highest resolutions (Stein et al., 2014, Nicol et al., 2015). This is thought to be  
81 due to the scheme not correctly representing the partially resolved turbulence. The role of the  
82 subgrid mixing scheme is to represent the turbulence which is not resolved but this balance is,  
83 overall, not producing enough turbulence. The behaviour is therefore sensitive to the subgrid  
84 mixing scheme used and so the development of suitable schemes is of prime importance.

85 There has also been similar work to investigate the behaviour of partially resolved turbulence  
86 in convective boundary layers – in particular the transition from high resolution LES  
87 simulations to lower resolution mesoscale simulations (Efstathiou et al., 2015). Efstathiou et  
88 al., 2016) compared the representation of morning boundary layer development in 50m LES  
89 with two grey zone boundary layer implementations at lower resolutions (down to 3200m).  
90 They evaluated the resulting deficiencies in either evolution of TKE or the amount of  
91 instability in the profiles and concluded that both formulations have strengths and weaknesses  
92 which highlights the inevitable issues with resolutions that are currently computationally  
93 feasible. Ching et al., (2014) investigated the generation of convectively induced secondary  
94 circulations in models of various gridlengths and showed that these are incompatible with  
95 parameterised boundary layer schemes. Miao et al., (2008) looked at the boundary layer  
96 structure over Beijing in a 500m grid-length WRF model with particular emphasis on the

97 formation of Horizontal Convective Rolls (HCRs) over the urban area. Of relevance to the  
98 current paper they concluded that HCRs are more likely over urban areas due to shear  
99 produced by the rough surface.

100 This work uses observations of turbulence in a dry, cloudless convective boundary layer case  
101 in London to understand the impact of resolution and domain size on simulated urban  
102 convective overturning in 100m and 50m gridlength models running in LES mode. These  
103 aspects were chosen for detailed study due to their practical importance for future city scale  
104 models. This paper assesses how physically realistic the convective structures appear to be by  
105 comparison with observations and theory. Spectral analysis is used to understand the effects  
106 of varying the model resolution. Conclusions are drawn about spin up effects at model  
107 boundaries and the development of the convective urban boundary layer as it grows across  
108 the city.

## 109 **2. Model, observational and case details.**

### 110 **2.1 Models**

111 The MetUM, version 5.2 onwards, solves non-hydrostatic, deep-atmosphere dynamics using  
112 a semi-implicit, semi-Lagrangian numerical scheme (Davies et al., 2005). The model includes  
113 a comprehensive set of parameterisations, including boundary layer (Lock et al., 2000) and  
114 mixed-phase cloud microphysics (Wilson et al., 1999). Although the model contains an  
115 option for convection parameterisation this is switched off in the configurations described  
116 here. Of importance to the work described here is the surface scheme which is JULES (Best,  
117 M et al., 2011). As part of this surface scheme the models used in the current work  
118 incorporated a one tile urban scheme described by Best (2005). This scheme sometimes  
119 results in a lag in warming up of urban surfaces in the morning (King and Bohenstengel pers.  
120 comm. 2015, Finnenkoeter pers. comm. 2018) but was used here because it was the scheme

121 in operational use at the time of this work. The model runs on a rotated latitude/longitude  
122 horizontal grid with Arakawa C staggering and a terrain-following hybrid-height vertical  
123 coordinate with Charney-Philips staggering. The standard level set as used in the UKV model  
124 has 70 levels in the vertical up to the model top at 40 km. In order to increase the resolution  
125 in the boundary layer, the distribution of the levels near the ground is quadratic so, for  
126 example, there are 16 levels in the lowest 1km of the atmosphere.

127 For the research reported in this paper a nested set of model configurations were run with  
128 MetUM version 8.1 as detailed in Figure 1 and table 1. A 500m grid-length model covering  
129 southern and central England was one way nested within the UKV model. The UKV is a  
130 1.5km grid-length UK model used for operational forecasting. The “V” in the name UKV  
131 refers to the fact that a variable resolution grid is used with lower resolution around the  
132 outside. As discussed by (Tang et al., 2013) the variable resolution enables a larger domain to  
133 be used a lower cost to avoid boundary spin up effects in the area of interest. Nested in the  
134 500m model was a 100m model centred on London with an 80kmx80km domain henceforth  
135 referred to as U100. This was the largest domain that it was thought practical to run due to  
136 computational constraints. In order to further understand the effects of resolution a 50m  
137 model, U50, was also run over the same area as U100 and also nested in the 500m model. In  
138 order to investigate spin up effects at model boundaries, we also present some results from a  
139 100m model with the same configuration and also centred on the same point in central  
140 London but running on a smaller 30 km x 30 km domain, referred to as U100S. Although  
141 1.5km and 500m models were run as part of the set of nested models, results from them are  
142 not reported since they are too coarse grid-length to explicitly represent the convective  
143 overturning which is the subject of this paper.

144 The model configurations were the same as that used for work on convection at similar  
145 resolutions (Hanley et al., 2015) and are summarised in Table 1. Apart from grid-length

146 dependent changes such as timestep and solver tolerance the main difference with resolution  
147 was a switch over from using 2D Smagorinsky mixing with the vertical mixing being carried  
148 out by the boundary layer scheme in the UKV to using 3D Smagorinsky ( $c_s=0.2$ ) in the  
149 500m,100m and 50m grid-length configurations. It should be noted that more recent UM  
150 configurations a scale aware blending scheme is used which blends between the boundary  
151 layer scheme and 3D Smagorinsky according to the ratio of boundary layer height and grid-  
152 length (Boutle et al., 2014). This was not used here because it was thought that using 3D  
153 Smagorinsky would be a cleaner test of the model in LES mode. In addition, in convective  
154 boundary layer situations such as investigated here, one would expect the blended scheme to  
155 operate in the 3D Smagorinsky limit in order 100m grid-length models. The 500m,100m and  
156 50m grid-length configurations used a 140 level set in the vertical which consisted of the  
157 standard 70 level set doubled all the way up. The orography and land use data were based on  
158 100m and 25m datasets respectively and became more detailed in the 500m, 100m and 50m  
159 grid-length models commensurate with the resolution. The land use dataset used was the ITE  
160 dataset (Bunce et al 1990). The urban fraction in the land use data in U100 is shown in Figure  
161 1 – at this scale many neighbourhood scale features of the city including parks and the river  
162 can clearly be seen.

## 163 **2.2 Observations.**

164 The observations used here were obtained from the ACTUAL project (Lane et al., 2013,  
165 Barlow et al., 2015, Halios and Barlow, 2018) measurement sites in London: the BT Tower  
166 (lat.  $51^{\circ} 31' 17.6''$  W lon.  $0^{\circ} 08' 20.36''$  N) and the Westminster City Council (WCC) roof-  
167 top site (lat.  $51^{\circ} 31' 16.31''$  N lon.  $0^{\circ} 09' 38.33''$  W). The BT Tower is the tallest building  
168 within several kilometres, with good exposure to winds in all directions. Within 10 km of the  
169 BT Tower the land surface cover is a mixture of residential and commercial with a mean  
170 building height of  $8.8 \pm 3$  m, roughness length within central London is estimated to be 0.87

171  $\pm 0.48$  m, and the displacement height  $4.3 \pm 1.9$  m (Wood et al., 2010). There are two large  
172 parks nearby: Regent's Park ( $1.66 \text{ km}^2$ ) approximately 0.64 km north-west of the Tower;  
173 Hyde Park ( $2.53 \text{ km}^2$ ) approx. 1.7 km to the south-west. It should be noted that the source  
174 area for the BT Tower is approximately 2-3 km in scale in convective conditions, 10-20 km  
175 in neutral (Helfter et al., 2011), and represents a mixture of urban and vegetative surfaces.

176 Two identical instrumentation platforms were used for turbulent flux measurements as fully  
177 described in Barlow et al. (2015). In this paper, only data from the sonic anemometer on top  
178 of the BT Tower were used (Gill Instruments R3-50). The head of the sonic anemometer was  
179 placed at 190 m a.g.l. on the BT Tower, the instrument being clamped to a pole on the top of  
180 an open lattice scaffolding tower of 12.3 m height on top of the main structure, meaning that  
181 the sensor head was 0.76 m higher than the lattice. A full description of the lattice is given in  
182 Barlow et al. (2011), where it was deduced from wind tunnel tests that there is only slight  
183 flow distortion at the height of the sensor due to the lattice. The sonic anemometer was  
184 sampled at 20 Hz.

185 A heterodyne Doppler lidar (Halo-Photonics "Streamline") with scanning capability was  
186 installed on the roof-top of the WCC site to measure the vertical structure of the urban  
187 boundary layer. The instrument operated at  $1.5 \text{ }\mu\text{m}$  wavelength; the pulse repetition  
188 frequency was 20 kHz, with integrated signals being output every 3.6 s; the sampling  
189 frequency was 30 MHz, and the return signal was resolved into 30 m long range gates.

190 Within the first three gates of the lidar (90m), returns were of insufficient quality; therefore  
191 results are presented from the fourth gate upwards, mid-gate height being 124 m a.g.l. once  
192 the height of the WCC building at the location of the lidar is taken into account.

193 Two modes of operation were used: a) continuous stare mode (pointing vertically) and b)  
194 Doppler Beam Swinging (DBS) mode for measuring the vertical wind profile (Lane et al.

2013). The DBS mode sampled in three orthogonal directions: vertically, tilted  $15^\circ$  off-zenith  
to east and to north. The DBS scan cycle lasted approximately 21 s, the time interval between  
the start of scans in DBS mode was 120 s, and the lidar was in vertical stare mode in the  
intervening 99 s. Hourly-averaged profiles of vertical velocity variance,  $\sigma_w^2(z)$ , were  
derived from the vertical stares. Due to the limited sampling rate a spectral correction was  
applied according to Barlow et al. (2015). Whereas boundary layer height is often defined as  
the height of the capping inversion in convective conditions, the mixing height,  $z_{MH}$ , is the  
depth of the layer adjacent to the ground over which pollutants become dispersed by  
turbulence (Seibert, 2000). Mixing height was estimated from the corrected variance profiles  
by applying a simple threshold method: the mixing height was taken as the gate up to which  
 $\sigma_w^2(z) > 0.1\text{m}^2\text{ s}^{-2}$ . To account for uncertainty in the choice of threshold, its value was  
perturbed by 21 steps of up to  $\pm 30\%$ , and the resulting mean was taken as  $z_{MH}$ , and  
maximum and minimum values were taken as the uncertainty bounds (Barlow et al. 2015).

To estimate the spectral energy density for the lidar a spectral splicing technique was used  
(Kaimal and Finnigan, 1994). As the lidar switched between two different scanning modes  
(vertical stare and DBS), the observed time series of vertical velocity,  $w$ , was discontinuous.  
The lidar  $w$  observations over a 2-hour period were split into two sets. The first set consisted  
of  $\sim 60$  short records taken in vertical stare mode, each with  $\sim 28$  samples approximately every  
3.6 seconds from which the high frequency part of the spectrum was estimated by applying a  
Fourier Transform. Spectra were averaged to give a single high-frequency spectrum. A  
second set was made up of 240 non-overlapping block averages (each block containing 30 s  
of data) from which the low frequency part of the spectrum was estimated. Then the high and  
low frequency parts of the spectrum were combined and smoothed. The splicing method was  
tested on the continuous, BT Tower sonic anemometer time series by sampling it in a similar

219 way to the lidar and the resulting spectrum was found to agree well with the continuous data  
220 spectrum in magnitude.

221

## 222 **2.3 The case.**

223 Model behaviour has been analysed for the case of the 30th September 2011. This was the  
224 middle of a period of five warmer than average and completely cloud free days in the London  
225 area (28<sup>th</sup> Sept – 2<sup>nd</sup> Oct). These conditions were a result of high pressure to the east of the  
226 UK. This case has been studied by J F Barlow et al., (2015) as a strong Urban Heat Island  
227 event. An important aspect of the case for subsequent analysis is that there is a significant  
228 synoptic flow from the south. Data from the lidar situated at WCC shows that the boundary  
229 layer grows in depth during the morning, with convective overturning from approximately  
230 1100 to 1600 UTC with this being deepest and most intense from 1400 to 1500 UTC (figure  
231 4).

## 232 **3. Overview of behaviour of model compared to observations**

233 In this section we present some basic behaviour of the models and comparisons between the  
234 models and observations which serve as a starting point for the analysis in sections 4 and 5.

235 Figure 2(a) shows the 1.5m temperature field in U100 at 1400 UTC. The city is clearly  
236 warmer and some fine scale detail can be seen (e.g. parks and rivers colder) reflecting the  
237 high resolution surface information in the model. The cooler approximately east-west line to  
238 the south of the figure is the ridge of a range of hills (the North Downs). Figure 2(b) shows  
239 the vertical velocity field at 293m above the ground. Comparing with Figure 2(a) it is clear  
240 that there is stronger overturning over the densely urban areas around the centre of London.  
241 The other feature, which is noticeable, is that the morphology of the overturning is strongly

242 influenced by the southerly wind with many linear/elongated features being aligned roughly  
243 along the flow. Such Horizontal Convective Rolls (LeMone, 1973) are common in sheared  
244 convective boundary layers and it was suggested by Miao and Chen (2008) that they might be  
245 common over urban surfaces where shear stress is higher. There are also signs of more  
246 elongated features, in particular close to the inflow (southern) boundary of the domain.

247 Figure 3 introduces two key aspects of model behaviour, which will be the subject of later  
248 sections of this paper. Figure 3(a) shows the horizontal vertical velocity field in U100 over  
249 the subset of the domain that corresponds to the small 100m model. Figure 3(b) shows the  
250 same field in the same subset of U50. It is noticeable to the eye that the features in the  
251 vertical velocity field are smaller (both the width of the streaks of high vertical velocity and  
252 their spacing). This immediately implies that the model is not converged in this respect. It is  
253 important to understand the effects of this because of the practical question of at which grid-  
254 length the model needs to be run for different applications. This aspect is discussed further in  
255 Section 4. Figure 3(c) shows the whole domain of U100S. It is clear that there are significant  
256 spin up effects as the air enters through the southern boundary of the model. These manifest  
257 themselves as an area close to the boundary where there is no overturning (because the  
258 driving model does not support it) but further into the model elongated along wind Horizontal  
259 Convective Rolls (HCRs) are generated. Further downstream again (roughly north of an east-  
260 west line half way between the north and south boundaries) the rolls become less coherent  
261 and look more like the elongated features in the subset of the larger domain. The formation of  
262 these rolls is discussed in Section 5 along with the practical implications of this spin up which  
263 clearly extends about 15km into the domain in this case. The location of the measurements is  
264 shown on Figure 3 (c) and was at the downstream end of the HCRs where they are starting to  
265 break up.

266 Figure 4 shows time/height cross sections of vertical velocity at the location of the lidar.

267 Figure 4(d) shows the vertical velocity from the lidar observations which show overturning in  
268 the mixed layer which deepens rapidly after 1200 UTC. The equivalent U50 and U100 data  
269 (Figures 4c and 4b) show similar overturning with, by eye, both the depth of the overturning  
270 and its magnitude in reasonably good agreement with the observations. The magnitude of the  
271 overturning appears somewhat weaker in the model and the frequency at which the  
272 overturning happens appears somewhat slower in the models and slower in U100 compared  
273 to U50. These comparisons of the model with observations are analysed more quantitatively  
274 below. U100S has similar overturning but at a much lower frequency and is clearly in poorer  
275 agreement with the observations. This is empirically understandable in the sense that if there  
276 are HCRs in the along wind direction in U100S (as shown in Figure 3) they would tend to  
277 advect along their length and so not change very rapidly when seen from a fixed point.

278 Figure 5 shows profiles of sensible heat flux in the U100 and U50 including the explicit  
279 fluxes corresponding to the explicit vertical velocities and the parameterised heat flux from  
280 the boundary layer scheme. The fluxes were calculated over a box 5x5km square centred at  
281 the BT Tower location. The explicit fluxes were calculated at a fixed time (1400 UTC) using  
282 the variations in potential temperature and vertical velocity across the box for each model  
283 level. In both models the flux is primarily carried explicitly except for close to the ground. As  
284 would be expected the U50 has the explicit flux increasing more quickly above the ground.

285 Both profiles show a large entrainment peak at around 650m. This is consistent with the  
286 morning increase in the mixed layer height with time and also as the air flows over the urban  
287 area with higher heat fluxes.

288 Figure 6(a) shows profiles of vertical velocity variance calculated at the location of the lidar  
289 in the time domain from 1400-1500 for the U100, U50 and the lidar data. It is clear that the  
290 models both have significantly lower vertical velocity variance than is observed but with this

291 error smallest at the lowest levels. The low values of variance at low levels are probably a  
292 manifestation of being under-resolved (as discussed in section 5). It is notable that U50 has  
293 higher variance than U100 below 300m (where the comparisons with the BT tower in section  
294 4 are made) but the variance is lower than U100 above that. U100 has a clear sign of a double  
295 structure with two separate peaks which can be seen by eye in figure 3 (as two separate levels  
296 at which the vertical velocity features tend to be centred). Figure 6(b) shows a horizontally  
297 averaged theta profile which shows that the double structure in the model corresponds to a  
298 stable layer around 700-900m altitude with a second less stable region above. It is notable  
299 that the variance in U50 is much lower than that in U100 in the region of the more elevated of  
300 the two peaks, to the degree that U50 doesn't have the peak at all.

301 Figure 7 shows the mixing height,  $z_{MH}$ , at the WCC measurement site as a function of time  
302 derived using a vertical velocity variance threshold of  $0.1 \text{ m}^2 \text{ s}^{-2}$  applied to both the lidar and  
303 model data. The error bars correspond to perturbing the threshold by  $\pm 30\%$ . It should be  
304 noted that earlier in the day, the explicit vertical velocity variance in the model does not reach  
305  $0.1 \text{ m}^2 \text{ s}^{-2}$  at any height, and thus  $z_{MH}$  could not be derived according to this threshold.  
306 However, from 1300 to 1500 UTC agreement is reasonably good for U100 although it is clear  
307 from the variance profiles shown in Figure 6(a) that the value of  $z_{MH}$  derived for the models  
308 will depend more strongly on the threshold chosen than in the case of the lidar. The  
309 somewhat lower value of  $z_{MH}$  derived for U50 reflects the lack of variance seen in Figure 6(a)  
310 in the elevated area of overturning from about 1000-1300m. This may result from the heat  
311 fluxes being somewhat lower than in reality due to the deficiencies in the surface exchange  
312 scheme in the model mentioned in section 2.1. The U100 model, in contrast has more  
313 significant variance between 1000-1300m because some of the larger scale structures are  
314 more energetic as can be seen in Figure 4.

315

## 316 **4. Spectral behaviour and effect of resolution**

317 In this section the effect of model resolution is analysed with comparisons between the  
318 spectra and turbulent lengthscales of U50, U100 and observations. As discussed above, figure  
319 3 shows that the model vertical velocity fields are different at 50m compared to 100m grid-  
320 length with smaller horizontal scales appearing in the vertical velocity structures. In addition  
321 figure 4 shows that the overturning appears to be faster in the U50. In order to better  
322 understand these aspects, spectral analysis has been carried out. Figure 8 shows spectra of  
323 timeseries of vertical velocities,  $w$ , for the 14-16UTC time window. The figure includes  
324 spectra of  $w$  from the sonic anemometer on the BT Tower (height 190 m), the nearest lidar  
325 gate (mid-point 184 m) and model spectra calculated for the nearest model level (midpoint  
326 height 192 m) and gridpoint. The spectral energy density has been multiplied by the  
327 frequency to highlight the most energetic scales.

328 The sonic anemometer spectra from the BT Tower and the lidar data agree that the peak  
329 frequency is around  $2 \times 10^{-3}$  Hz although there is somewhat less energy in the lidar spectrum.  
330 This difference is discussed by Barlow et al., (2015) and is thought to be related to the  
331 differences in sampling frequency, sampling volume and location of the two instruments. The  
332 U50 and U100 spectra have similar peak magnitude of scaled spectral energy density  
333 compared to the observations. As variance is given by integrating the spectral energy density  
334 with frequency the spectra are consistent with this in that the variance at 190m in figure 6 is  
335 higher in U50. There is a sharp drop-off in energy at higher frequencies due to the finite  
336 resolution of the model. This starts near the peak frequency for U50, and is below the peak  
337 frequency for U100. U50 therefore is close to resolving the dominant frequency whereas  
338 U100 only partially resolves the peak. This is consistent with the finding that, in the spatial  
339 domain, the spacing of the high vertical velocity features appears to reduce between U100

340 and U50 which means that U100 is not completely resolving the structures. It is also  
341 consistent with the variance data shown in Figure 6 where U50 is closer to having the  
342 observed variance at 190m. By comparison, Miao et al., 2008) used the WRF model running  
343 with 500m grid-length over Beijing and found HCRs of a smaller aspect ratio than for rural  
344 boundary layers: it is possible that their structures were under-resolved. The implication is  
345 that, with the MetUM, a grid-length of about 50m is required to resolve the most important  
346 spatial/temporal structures in this convective boundary layer although, as shown in figure 5,  
347 100m may still be sufficient if we are only concerned with bulk properties such as heat flux  
348 averaged across a certain distance. The numbers quoted in the previous sentence will be  
349 different with different models with different dynamical cores. From figure 8 we can also  
350 estimate what the spectra for hypothetical 25m and 12.5m models would look like assuming  
351 that each factor of two resolution will again give a factor of two increase in the frequency at  
352 which the model energy drops off from the observational data. A 25m model would more  
353 comfortably resolve the most energetic frequencies and we might expect more convergence  
354 in the comparison with observations at shorter grid-lengths than this. This is based only from  
355 extrapolating what we see in the spectra of the 100m and 50m models so experiments at 25m  
356 and also probably at 12.5m would be needed to confirm this conclusion.

357 Given the nature of the observational data (time series in one location) the spectra discussed  
358 above were computed in the time domain. As a check we also calculated a spectrum for U50  
359 in the space domain from the horizontal field along the transect. If the spatial frequencies in  
360 this spectrum are converted into temporal ones using the wind velocity (about  $6\text{ms}^{-1}$  at BT  
361 Tower level) the spectrum (not shown) looks very similar to the U50 one in figure 8. This  
362 implies that the behaviour of the time spectrum is dominated by advection of spatial features  
363 rather than the temporal changes in these. This fits with the observation that the drop off in  
364 the U100 and U50 spectra occur at about a factor of 2 different frequency which corresponds

365 in the difference in spatial resolution (whereas, as shown in table 1, the timestep is a factor of  
366 3 different). If converted to a lengthscale with the wind velocity the frequency at which the  
367 model curve starts to strongly drop away from observed values (around  $2 \times 10^{-2} \text{s}^{-1}$   
368 corresponding to 50s for U100) corresponds to a length of around 6 grid-lengths using the  
369 advection speed mentioned above. This is the magnitude of filter scale typically seen in NWP  
370 models (Lean et al., 2003). In contrast in the temporal domain the same frequency at which  
371 the model starts to be attenuated is much lower (50x) than the Nyquist frequency due to the  
372 timestep,  $1.0 \text{s}^{-1}$ . This implies that the model is running with a shorter timestep than needed to  
373 resolve this convective overturning. In practice it is found that this short a timestep is  
374 required for the model to be numerically stable but this requirement may well not come from  
375 the boundary layer in the centre of the domain. It could come, for example, from higher up in  
376 the model (which extends to 40km) or from the region of the boundaries.

377 The analysis above applies to only one level, 190m above ground, which is where the BT  
378 tower measurements were taken. However, the lidar data also allows spectra to be calculated  
379 at a number of heights, and a dominant time-scale,  $\Lambda_t$ , can be estimated from the frequency of  
380 the peak. The spectral energy peak was estimated by fitting a second-order polynomial  
381 (Wood et al. 2010). The dominant length-scale  $\Lambda_x = U \Lambda_t$  was calculated at each height using  
382 the observed hourly mean wind profile,  $U(z)$ . The same calculation was done for the model  
383 spectra, using wind profiles spatially averaged over a 10km box around the observation site.  
384 Fig. 9 shows the height-normalised profile of dominant lengthscales, all of which have been  
385 scaled using  $z_{MH}$  for lidar and model data. The empirical relationship due to Caughey and  
386 Palmer (1979) (CP) has also been added as a reference for a classical Convective Boundary  
387 Layer. The general trend of the lidar data follows the CP relationship, and the magnitude is  
388 slightly smaller but with two large peaks superimposed. The two peaks are consistent with  
389 the double structure in the overturning discussed in section 3. The models both have longer

390 lengthscales than the lidar observations which corresponds to the limited resolution as  
391 discussed above. Closer to the ground the models have larger scales relative to the  
392 observations. The resolution effect is clear in that the U100 data generally has a larger  
393 lengthscale than U50. U50 shows a weak double peak structure whereas U100 shows a single  
394 lower peak which is lower than the peaks in the observations. These results demonstrate  
395 again that U50 is producing near-realistic convective structures and even U100 is producing  
396 structures that are only 2-3 times the expected scale at a height of around  $z_{MH}/2$ .

397

## 398 **5. Horizontal behaviour and spin up.**

399 It is also of interest to look at the spatial distribution of some of the quantities discussed in  
400 section 3. Although we do not have any observational data on horizontal variability it is  
401 important to understand the effect of the city surface and spin up at the edge of the model  
402 domain.

403 Figure 10 shows a cross section of instantaneous vertical velocity at 1400 UTC U100. The  
404 cross section is along a transect from south to north, i.e. aligned with the wind, across the  
405 U100 domain passing through the location of the BT tower (i.e. along the dotted line shown  
406 in figure 3c). The overturning can be clearly seen and it behaves as would be expected with  
407 the depth of the overturning increasing as the air flows over the built up area of London and  
408 decreasing again downstream of the city. This is summarised in Figure 11(a) which shows the  
409 mixing height (solid line) calculated from a spatial variance threshold of  $0.1 \text{ m}^2\text{s}^{-2}$  along with  
410 the model urban fraction averaged over gridpoints in a 5km box surrounding each point. It is  
411 striking that the mixing height is very flat over the city despite the fact that the urban fraction  
412 and surface heat flux (not shown) both have peaks corresponding to the centre of the city.  
413 This is assumed to be because of a synoptically imposed inversion (which can be seen from

414 the potential temperature ( $\theta$ ) contours in figure 10 and figure 6b) which caps the height of  
415 the overturning. Figure 10 shows evidence of the double structure in the vertical as seen in  
416 the variance values (Figure 6) - vertical velocity features can be seen which are centred in the  
417 vertical at relatively low levels ( $\sim 400\text{m}$ ) while others are evident higher up ( $\sim 1000\text{m}$ ). The  
418 sudden reduction of the depth of overturning at 60km on the transect visible in figures 10 and  
419 11a which subsequently recovers before 80km may be partly due to a region of a relatively  
420 low inversion at around 600m visible in the  $\theta$  field.

421 It is important to understand spin up effects at the edge of the domains and, in particular, how  
422 far they extend into the domain. Given the expense of running high resolution models it is  
423 important not to run domains larger than are strictly required for the application for which  
424 they are intended.

425 The discussion around Figure 3 introduced the elongated roll structures, HCRs, aligned along  
426 the wind direction, when air flows into the domain of U100S. Similar, but less pronounced,  
427 HCRs may also be seen near the inflow boundary of U100 (Figure 2b). HCRs such as this can  
428 be valid meteorological phenomena (e.g. when generated as air comes over a coast or other  
429 physical boundary) but are very likely to be spurious when generated by the boundary of a  
430 model. The boundary conditions of the 100m grid-length models come from a lower  
431 resolution model (500m) which are only updated every 15 minutes. It would therefore not be  
432 possible for explicit overturning in the boundary layer to be propagated into the model from  
433 the boundaries. This results in a region of no overturning close to the boundary, followed by  
434 the HCRs further into the domain which then break up into more realistic looking structures  
435 further downstream. These effects represent spin up as the behaviour of the modelled air  
436 adjusts to the high resolution. HCRs due to spin up at the inflow boundary have been seen in  
437 a number of contexts in turbulence permitting models (Boutle et al., 2014, Hanley et al.,  
438 2015). In this section we analyse why these rolls are seen.

439 In order to quantify the spin up effects, Figure 12 shows an analysis of the aspect ratio of  
440 objects in the vertical velocity field on the 290m model level with the objects being defined  
441 as contiguous areas with vertical velocity greater than  $2\text{ms}^{-1}$ . The aspect ratio was calculated  
442 using a least squares method to fit an ellipse to each object and then determine the aspect  
443 ratio as the ratio of major to minor axis of the fitted ellipse. For each object in the whole  
444 domain the aspect ratio and distance from the inflow (southern) boundary was calculated.  
445 The aspect ratio was then plotted as a function of distance from the boundary with some  
446 smoothing (moving box of 30 gridpoints which corresponds to 3km). The figure shows that,  
447 in U100, even in the centre of the domain the high vertical velocity objects are somewhat  
448 elongated with average aspect ratio around 3.0 (as can be seen by eye in figure 3a). In that  
449 model there is a clear tendency for more elongated objects close to the inflow boundary with  
450 average aspect ratio increased to around 6.0. However, the curve U100S shows much more  
451 elongated cells with the average aspect ratio peaking at nearly 10.0. It is clear that the spin up  
452 effect in terms of HCRs is more pronounced when the boundary of the domain is closer to the  
453 region with strong overturning.

454 In order to understand this in more detail an analysis based on the boundary layer stability  
455 parameter is presented. Salesky et al., (2017) carried out LES studies of the transition between  
456 roll and cellular organisation in convective boundary layers. They found that the transition  
457 could be described by a stability parameter,  $-z_i/L$  where  $z_i$  is the inversion height and  $L$  is the  
458 Obukhov length. We assume that  $z_i = z_{MH}$  at the time of the analysis (1400 UTC) in the  
459 middle of the day. It was found that the transition takes place at around  $-z_i/L = 10$  with  
460 smaller values of  $-z_i/L$  giving more roll like structures and higher values more cellular. In  
461 this case we do not see cells due to the relatively strong synoptic flow, however we are  
462 interested in the transition between HCRs and more discrete (although still somewhat  
463 elongated) objects. It should be noted that the same 100m model does produce cellular

464 structures in convective boundary layers for other cases where there are much lighter winds  
465 (not shown).

466 Figure 11 shows the results for calculating the stability parameter along the same south-north  
467 transect used in figure 10. All quantities in this figure are averaged over 5km boxes centred  
468 on points along the transect. Figure 11(a) shows the mixing height calculated as a variance  
469 threshold for both the 100m and the small 100m models. In the small model the mixing  
470 height starts very small at the southern boundary but increases rapidly as the air transits the  
471 model domain. This is consistent with convection being driven by surface fluxes and so the  
472 overturning grows upwards from the surface once the air enters a model that is able to  
473 support it. Figure 11(b) shows the Obukhov Length,  $L$ , for both models. This was calculated  
474 (assuming unstable conditions) as  $L=z/R_i$  (Businger et al., 1971) where  $R_i$  is the gradient  
475 Richardson number in the surface layer given by:

$$476 \quad Ri = \frac{g \frac{\partial \bar{\theta}}{\partial z}}{\bar{\theta} \left( \frac{\partial \bar{U}}{\partial z} \right)^2}$$

477  $R_i$  was calculated from the model data by fitting logarithmic polynomials to the smoothed  
478 (lengthscale 5km)  $\theta$  and  $U$  profiles using the lowest 5 model levels (up to about 20m) and  
479 then using the fitted profiles to calculate the vertical derivatives. When the stability  
480 parameter,  $-z_{MH}/L$ , is calculated (figure 11c) the value is much lower in U100S, close to the  
481 southern boundary, than in U100, which is consistent with rolls being more prominent in  
482 U100S in that location. As the northern boundary of U100S is approached, the values are  
483 almost the same which implies that, by this point, the spin up effects are no longer important.  
484 Figure 11 also gives some insight into the reasons for this. Figure 11b shows the Obukhov  
485 length along the transect. It is noticeable that  $L$  is small north of 65km on the transect despite  
486 the fact that the heat flux would be expected to be lower outside the urban area. This is

487 consistent with the low level shear being lower in this area as can be seen on cross sections of  
488 the wind strength (not shown). The values of the Obukhov length are similar between the  
489 small and large models along the whole part of the transect that is inside the small model  
490 domain. Most of the difference in the stability parameter appears, therefore, to come from the  
491 difference in the mixing height. The boundary layer is more shear dominated in U100S near  
492 the boundary because it is shallower.

493 It is also noticeable in figure 11c that the stability parameter is also small near the boundary  
494 of U100 and that there is likely to be a similar spin up distance. This can be seen by eye in the  
495 vertical velocity fields (e.g. figure 2b) although the rolls are much weaker due to the lower  
496 surface heat flux outside the city.

497 Beyond the spin up zone it is striking to note that from 20-40 km, the Obukhov length  
498 remains near constant despite a large increase in urban fraction, as concurrent increases in  
499 both sensible heat flux and surface stress towards the city centre produce little overall change  
500 in surface layer stability. Together with the near constant mixing height over this zone, the  
501 boundary layer stability also remains near constant. The aspect ratio of convective structures  
502 stays fairly constant, reducing only slightly over 40-60km as the boundary layer stability  
503 parameter drops. The surprise is that the convective field remains relatively invariant despite  
504 massive changes in the urban surface, although this particular combination of increasing  
505 surface stress and heat flux might be peculiar to London, and the strong capping inversion  
506 across the region at the time.

507 Figures 3, 11 and 12 show that the spin up effects penetrate at least 10-15km into the domain  
508 of the U100S in this case although this distance will depend on the wind strength. It is  
509 interesting to note that in the spectral analysis in the section 4 the dominant timescale of the  
510 overturning, from the peak of the spectrum of the U100 in figure 8 is approximately 500s. If

511 one assumes the wind speed is about  $10\text{ms}^{-1}$  (representative of the middle of the boundary  
512 layer) this means that the spin up distance corresponds to 2-3 turnover times which seems  
513 intuitively reasonable. U50 would be expected to have a somewhat shorter dominant  
514 timescale from better resolving the peak in the observed spectrum and would therefore spin  
515 up more quickly (although slower in terms of number of gridpoints). It is important to note  
516 that while we have analysed these effects in terms of the stability parameter the details of  
517 how far the spin up penetrates into the domain will depend on the model numerics and the  
518 sub-grid mixing configuration employed. The effect of these two aspects of models on  
519 convective structures were analysed in terms of an effective viscosity by Piotrowski et al.,  
520 2009.

521 As shown in figure 4, these spin up artefacts can significantly degrade the model performance  
522 compared to observations. This is an important issue for practical models with these  
523 resolutions. The simple solution of simply extending the domain is not always feasible due to  
524 the computational expense. One approach which was employed by Vosper et al., (2013) is to  
525 use a variable resolution model. The benefits of variable resolution are discussed by Tang et  
526 al., (2013) and Davies, (2017) although not in the particular context of the turbulence  
527 permitting regime. The idea would be to extend the domain at lower resolution which can  
528 help to push the spin up region further away from the area of interest at lower expense than  
529 extending the domain at full resolution. A second possibility is to inject noise into the  
530 boundary data to help the turbulent motions spin up. Variations on this approach have been  
531 investigated by a number of workers including Muñoz-Esparza et al., (2014) and Mayor et  
532 al., (2002). There are also approaches to this issue that have been developed within the CFD  
533 community, for example running an auxillary model to model the inflow field as reported by  
534 Lund et al., (1998).

535 It is clear that the effects of spin up and how far it penetrates into the domain will vary  
536 greatly according to the meteorological situation and so the importance of this, and the need  
537 for mitigation, will depend on the application of the particular model. So, for example, a  
538 model whose primary aim is to forecast fog (as in Boutle et al., 2016) will generally be of  
539 greatest utility in relatively low wind situations so spin up effects would be likely to be less  
540 of an issue.

541

542

## 543 **6. Conclusions**

544 A comparison has been presented between  $O(100\text{m})$  grid-length versions of the MetUM over  
545 London and observations for a case of a cloud free convective boundary layer with a  
546 significant southerly wind. The boundary layer overturning is, in general, well represented in  
547 terms of the magnitude and depth of the overturning being in good agreement with vertical  
548 stare Doppler lidar observations of vertical velocity and the variation of these through the  
549 day.

550 An important practical question is the resolution requirements of the model. In order to help  
551 understand this the 100m model was compared to a 50m one. In both the 100m and 50m  
552 models most of the heat flux (except very close to the surface) is carried explicitly by  
553 overturning motions and is consistent between the two. This would imply that the turbulence  
554 is well resolved. In contrast, however, the comparison of the vertical velocity fields by eye  
555 reveals that the vertical features in the model are generally smaller in horizontal extent in the  
556 50m model which implies that the models have not converged with resolution as far as  
557 horizontal size of structures is concerned. Spectral analysis in the time domain has been  
558 carried out to compare the model to observations from an anemometer at the top of the BT

559 tower and from the lidar. The models both represent the most energetic eddies without too  
560 much attenuation but the 50m model represents significantly more frequencies higher than  
561 the peak. The exact details of the spectra of the model compared to observations are likely to  
562 depend on the model employed (dynamical core and sub-grid mixing) and the meteorological  
563 situation. Vertical profiles of integral lengthscales were calculated using the lidar and model  
564 data and showed that the most energetic eddies in the models are 2-3 times larger than the  
565 lidar, and worse close to the ground, which implies that higher resolutions would be  
566 preferable. The above indicates that, even at 50m resolution, the horizontal structures in the  
567 convective overturning are under-resolved in the model. However, if only bulk properties  
568 (e.g. heat fluxes, spatially averaged mixing height etc) are of interest models the implication  
569 of this study is that the 100m model will have usable performance. It would be interesting in  
570 future to extend the study to higher resolution models to see where convergence of the  
571 horizontal structures is reached. This was not possible in the current study due to  
572 computational constraints.

573 Although comparison with the available observations does not shed light on the spatial  
574 variation of the mixing height, this also looks reasonable in the model with a deeper mixing  
575 height over the more densely packed urban area in the centre of London. Comparison of the  
576 80x80km domain 100m model of the London area with a much smaller 30x30km domain  
577 model has allowed us to investigate spin up effects at the inflow boundary. These manifest  
578 themselves as along wind rolls just downstream of the inflow boundary which then break up  
579 approximately 10-15 km further downstream. In the case of the small model these rolls  
580 extend almost half way across the domain and cause significantly poorer agreement, in terms  
581 of temporal variation of vertical velocity, with the lidar vertical velocity observations. An  
582 analysis has been carried out based on a boundary layer stability parameter calculated as the  
583 ratio of the mixing height to the Obukhov Length. This implies that the formation of rolls is

584 primarily due to the small value of the mixing height near the inflow boundary (that  
585 subsequently increases downstream towards more physically realistic values), causing the  
586 boundary layer to be shear dominated. These spin up effects are likely to be an intrinsic  
587 property of these models and therefore may need to be avoided by using larger domains (or  
588 variable resolution) in order to push the area of interest further away from the boundary. An  
589 alternative approach may be to inject noise into the model via the boundaries in order to help  
590 the turbulence spin up more quickly.

591

592

## 593 **Acknowledgements.**

594 Observations were obtained under the ACTUAL project which was funded under  
595 Engineering and Physical Sciences Research Council grant number EP/G022938/1. The  
596 authors would like to thank Heather Guy for developing the ellipse fitting method used.

597 The authors would also like to thank the two anonymous reviewers whose comments helped  
598 improve the paper.

## **References**

- Allen, L., Lindberg, F., & Grimmond, C. S. B. (2011). Global to city scale urban anthropogenic heat flux: Model and variability. *International Journal of Climatology*, *31*(13), 1990–2005. <https://doi.org/10.1002/joc.2210>
- Barlow, J., Best, M., Bohnenstengel, S. I. S. I., Clark, P., Grimmond, S., Lean, H., ... Zhong, J. (2017). Developing a research strategy to better understand, observe, and simulate urban atmospheric processes at Kilometer to Subkilometer Scales. *Bulletin of the American Meteorological Society*, *98*(10), ES261-ES264. <https://doi.org/10.1175/BAMS-D-17-0106.1>
- Barlow, J. F., Halios, C. H., Lane, S. E., & Wood, C. R. (2015). Observations of urban boundary layer structure during a strong urban heat island event. *Environmental Fluid Mechanics*, *15*(2), 373–398. <https://doi.org/10.1007/s10652-014-9335-6>
- Barlow, J. F., Harrison, J., Robins, A. G., & Wood, C. R. (2011). A wind-tunnel study of

- flow distortion at a meteorological sensor on top of the BT Tower, London, UK. *Journal of Wind Engineering and Industrial Aerodynamics*, 99(9), 899–907. <https://doi.org/10.1016/j.jweia.2011.05.001>
- Best, M. J., M. P., Clark, D. B., Rooney, G. G., Essery, R. L. H., Menard C. B., ... Harding, R. J. (2011). The Joint UK Land Environment Simulator ( JULES ), Model Description - Part 1 : Energy and Water Fluxes The Joint UK Land Environment Simulator ( JULES ), model description – Part 1 : Energy and water fluxes, 677–699. <https://doi.org/10.5194/gmd-4-677-2011>
- Best, M. J. (2005). Representing urban areas within operational numerical weather prediction models. *Boundary Layer Meteorology*, 114, 91–109. <https://doi.org/10.1007/s10546-004-4834-5>
- Best, M. J., & Grimmmmond, C. S. B. (2015). Key conclusions of the first international urban land surface model comparison project. *Bulletin of the American Meteorological Society*, 96(5), 805–819. <https://doi.org/10.1175/BAMS-D-14-00122.1>
- Bohnenstengel, S. I., Evans, S., Clark, P. a., & Belcher, S. E. (2011). Simulations of the London urban heat island. *Quarterly Journal of the Royal Meteorological Society*, 137(659), 1625–1640. <https://doi.org/10.1002/qj.855>
- Bohnenstengel, S. I., Hamilton, I., Davies, M., & Belcher, S. E. (2014). Impact of anthropogenic heat emissions on London’s temperatures. *Quarterly Journal of the Royal Meteorological Society*, 140, 687–698. <https://doi.org/10.1002/qj.2144>
- Boutle, I. A., Eyre, J. E. J., & Lock, A. P. (2014). Seamless Stratocumulus Simulation across the Turbulent Gray Zone. *Monthly Weather Review*, 142(4), 1655–1668. <https://doi.org/10.1175/MWR-D-13-00229.1>
- Boutle, I. A., Finnenkoetter, A., Lock, A. P., & Wells, H. (2016). The London Model: Forecasting fog at 333 m resolution. *Quarterly Journal of the Royal Meteorological Society*, 142(694), 360–371. <https://doi.org/10.1002/qj.2656>
- Businger, J. A., Wyngaard, J. C., Izumi, Y., & Bradley, E. F. (1971). Flux-Profile Relationships in the Atmospheric Surface Layer. *Journal of the Atmospheric Sciences*. [https://doi.org/10.1175/1520-0469\(1971\)028<0181:FPRITA>2.0.CO;2](https://doi.org/10.1175/1520-0469(1971)028<0181:FPRITA>2.0.CO;2)
- Caughey, S. J., & Palmer, S. G. (1979). Some aspects of turbulence structure through the depth of the convective boundary layer. *Quarterly Journal of the Royal Meteorological Society*, 105(446), 811–827. <https://doi.org/10.1002/qj.49710544606>
- Chen, F., Kusaka, H., Bornstein, R., Ching, J., Grimmond, C. S. B., Grossman-Clarke, S., ... Zhang, C. (2011). The integrated WRF/urban modelling system: development, evaluation, and applications to urban environmental problems. *International Journal of Climatology*, 31(2), 273–288. <https://doi.org/10.1002/joc.2158>
- Ching, J., Rotunno, R., LeMone, M., Martilli, A., Kosovic, B., Jimenez, P. A., & Dudhia, J. (2014). Convectively Induced Secondary Circulations in Fine-Grid Mesoscale Numerical Weather Prediction Models. *Monthly Weather Review*, 142(9), 3284–3302. <https://doi.org/10.1175/MWR-D-13-00318.1>
- Clark, P., Roberts, N., Lean, H., Ballard, S. P., & Charlton-Perez, C. (2016). Convection-permitting models: A step-change in rainfall forecasting. *Meteorological Applications*, 23(2). <https://doi.org/10.1002/met.1538>

- Davies, T. (2017). Dynamical downscaling and variable resolution in limited-area models. *Quarterly Journal of the Royal Meteorological Society*, *143*(702), 209–222. <https://doi.org/10.1002/qj.2913>
- Davies, T., Cullen, M. J. P., Malcolm, A. J., Mawson, M. H., Staniforth, A., White, A. A., & Wood, N. (2005). A new dynamical core of the Met Office's global and regional modelling of the atmosphere. *Quarterly Journal of the Royal Meteorological Society*, *131*(608), 1759–1782. <https://doi.org/10.1256/qj.04.101>
- Efstathiou, G. A., & Beare, R. J. (2015). Quantifying and improving sub-grid diffusion in the boundary-layer grey zone. *Quarterly Journal of the Royal Meteorological Society*, *141*(693), 3006–3017. <https://doi.org/10.1002/qj.2585>
- Efstathiou, G. A., Beare, R. J., Osborne, S., & Lock, S. A. P. (2016). Grey zone simulations of the morning convective boundary layer development. *Journal of Geophysical Research*, *121*(9), 4769–4782. <https://doi.org/10.1002/2016JD024860>
- Halios, C. H., & Barlow, J. F. (2018). Observations of the Morning Development of the Urban Boundary Layer Over London, UK, Taken During the ACTUAL Project. *Boundary-Layer Meteorology*, *166*(3), 395–422. <https://doi.org/10.1007/s10546-017-0300-z>
- Hanley, K. E., Barrett, A. I., & Lean, H. W. (2016). Simulating the 20 May 2013 Moore, Oklahoma tornado with a 100-metre grid-length NWP model. *Atmospheric Science Letters*, *17*(8). <https://doi.org/10.1002/asl.678>
- Hanley, K. E., Plant, R. S., Stein, T. H. M., Hogan, R. J., Nicol, J. C., Lean, H. W., ... Clark, P. A. (2015). Mixing-length controls on high-resolution simulations of convective storms. *Quarterly Journal of the Royal Meteorological Society*, *141*(686). <https://doi.org/10.1002/qj.2356>
- Helfter, C., Famulari, D., Phillips, G. J., Barlow, J. F., Wood, C. R., Grimmond, C. S. B., & Nemitz, E. (2011). Controls of carbon dioxide concentrations and fluxes above central London. *Atmospheric Chemistry and Physics*, *11*(5), 1913–1928. <https://doi.org/10.5194/acp-11-1913-2011>
- Holt, T., & Pullen, J. (2007). Urban Canopy Modeling of the New York City Metropolitan Area: A Comparison and Validation of Single- and Multilayer Parameterizations. *Monthly Weather Review*, *135*(5), 1906–1930. <https://doi.org/10.1175/MWR3372.1>
- Honnert, R., Masson, V., & Couvreux, F. (2011). A Diagnostic for Evaluating the Representation of Turbulence in Atmospheric Models at the Kilometric Scale. *Journal of the Atmospheric Sciences*, *68*(12), 3112–3131. <https://doi.org/10.1175/JAS-D-11-061.1>
- Kaimal, J. C., & Finnigan J. J. (1994). *Atmospheric boundary layer flows—their structure and measurement*. Oxford University Press.
- Kendon, E. J., Roberts, N. M., Fowler, H. J., Roberts, M. J., Chan, S. C., & Senior, C. A. (2014). Heavier summer downpours with climate change revealed by weather forecast resolution model. *Nature Climate Change*, *4*(7), 570–576. <https://doi.org/10.1038/nclimate2258>
- Lane, S. E., Barlow, J. F., & Wood, C. R. (2013). An assessment of a three-beam Doppler lidar wind profiling method for use in urban areas. *Journal of Wind Engineering and*

- Industrial Aerodynamics*, 119, 53–59. <https://doi.org/10.1016/j.jweia.2013.05.010>
- Lean, H. W., & Clark, P. A. (2003). The effects of changing resolution on mesoscale modelling of line convection and slantwise circulations in FASTEX IOP16. *Quarterly Journal of the Royal Meteorological Society*, 129(592 PART A). <https://doi.org/10.1256/qj.02.57>
- LeMone, M. (1973). The structure and dynamics of horizontal roll vortices in the planetary boundary layer. *Journal of Atmospheric Science*, 30, 1077–1091.
- Leroyer, S., Bélair, S., Husain, S. Z., & Mailhot, J. (2014). Subkilometer numerical weather prediction in an urban coastal area: A case study over the vancouver metropolitan area. *Journal of Applied Meteorology and Climatology*, 53(6), 1433–1453. <https://doi.org/10.1175/JAMC-D-13-0202.1>
- Lock, A. P., Brown, A. R., Bush, M. R., Martin, G. M., & Smith, R. N. B. (2000). A New Boundary Layer Mixing Scheme. Part I: Scheme Description and Single-Column Model Tests. *Monthly Weather Review*, 128(9), 3187–3199. [https://doi.org/10.1175/1520-0493\(2000\)128<3187:ANBLMS>2.0.CO;2](https://doi.org/10.1175/1520-0493(2000)128<3187:ANBLMS>2.0.CO;2)
- Lund, T. S., Wu, X., & Squires, K. D. (1998). Generation of inflow data for spatially-developing turbulent boundary layer simulations. *Journal of Computational Physics*, 144, 233. [https://doi.org/DOI 10.1006/jcph.1998.5882](https://doi.org/DOI%2010.1006/jcph.1998.5882)
- Mayor, S. D., Spalart, P. R., & Tripoli, G. J. (2002). Application of a Perturbation Recycling Method in the Large-Eddy Simulation of a Mesoscale Convective Internal Boundary Layer. *Journal of the Atmospheric Sciences*, 59(1995), 2385–2395. [https://doi.org/10.1175/1520-0469\(2002\)059<2385:AOAPRM>2.0.CO;2](https://doi.org/10.1175/1520-0469(2002)059<2385:AOAPRM>2.0.CO;2)
- Miao, S., & Chen, F. (2008). Formation of horizontal convective rolls in urban areas. *Atmospheric Research*, 89(3), 298–304. <https://doi.org/10.1016/j.atmosres.2008.02.013>
- Miao, S., Chen, F., LeMone, M. a., Tewari, M., Li, Q., & Wang, Y. (2009). An Observational and Modeling Study of Characteristics of Urban Heat Island and Boundary Layer Structures in Beijing. *Journal of Applied Meteorology and Climatology*, 48(3), 484–501. <https://doi.org/10.1175/2008JAMC1909.1>
- Muñoz-Esparza, D., Kosović, B., Mirocha, J., & van Beeck, J. (2014). Bridging the Transition from Mesoscale to Microscale Turbulence in Numerical Weather Prediction Models. *Boundary-Layer Meteorology*, 153(3), 409–440. <https://doi.org/10.1007/s10546-014-9956-9>
- Nicol, J. C., Hogan, R. J., Stein, T. H. M., Hanley, K. E., Clark, P. A., Halliwell, C. E., ... Plant, R. S. (2015). Convective updraught evaluation in high-resolution NWP simulations using single-Doppler radar measurements. *Quarterly Journal of the Royal Meteorological Society*, 141(693). <https://doi.org/10.1002/qj.2602>
- Piotrowski, Z. P., Smolarkiewicz, P. K., Malinowski, S. P., & Wyszogrodzki, A. A. (2009). On numerical realizability of thermal convection. *Journal of Computational Physics*, 228(17), 6268–6290. <https://doi.org/10.1016/j.jcp.2009.05.023>
- Prein, A. F., Langhans, W., Fosser, G., Ferrone, A., Ban, N., Goergen, K., ... Leung, R. (2015). A review on regional convection-permitting climate modeling: Demonstrations, prospects, and challenges. *Reviews of Geophysics*, 53(2), 323–361. <https://doi.org/10.1002/2014RG000475>

- Ronda, R. J., Steeneveld, G. J., Heusinkveld, B. G., Attema, J. J., & Holtslag, A. A. M. (2017). Urban finescale forecasting reveals weather conditions with unprecedented detail. *Bulletin of the American Meteorological Society*, *98*(12), 2675–2688. <https://doi.org/10.1175/BAMS-D-16-0297.1>
- Salesky, S. T., Chamecki, M., & Bou-Zeid, E. (2017). On the Nature of the Transition Between Roll and Cellular Organization in the Convective Boundary Layer. *Boundary-Layer Meteorology*, *163*(1), 41–68. <https://doi.org/10.1007/s10546-016-0220-3>
- SMAGORINSKY, J. (1963). General Circulation Experiments With the Primitive Equations. *Monthly Weather Review*, *91*(3), 99–164. [https://doi.org/10.1175/1520-0493\(1963\)091<0099:GCEWTP>2.3.CO;2](https://doi.org/10.1175/1520-0493(1963)091<0099:GCEWTP>2.3.CO;2)
- Stein, T. H. M., Hogan, R. J., Clark, P. A., Halliwell, C. E., Hanley, K. E., Lean, H. W., ... Plant, R. S. (2015). The Dymecs project: A Statistical approach for the evaluation of convective storms in high-resolution NWP models. *Bulletin of the American Meteorological Society*, *96*(6). <https://doi.org/10.1175/BAMS-D-13-00279.1>
- Stein, T. H. M., Hogan, R. J., Hanley, K. E., Nicol, J. C., Lean, H. W., Plant, R. S., ... Halliwell, C. E. (2014). The three-dimensional morphology of simulated and observed convective storms over Southern England. *Monthly Weather Review*, *142*(9). <https://doi.org/10.1175/MWR-D-13-00372.1>
- Tang, Y., Lean, H. W., & Bornemann, J. (2013). The benefits of the Met Office variable resolution NWP model for forecasting convection. *Meteorological Applications*, *20*(4). <https://doi.org/10.1002/met.1300>
- Vosper, S., Carter, E., Lean, H., Lock, A., Clark, P., & Webster, S. (2013). High resolution modelling of valley cold pools. *Atmospheric Science Letters*, *14*(3). <https://doi.org/10.1002/asl2.439>
- Wilson, D. R., & Ballard, S. P. (1999). A microphysically based precipitation scheme for the UK Meteorological Office Unified Model. *Quarterly Journal of the Royal Meteorological Society*, *125*(557), 1607–1636. <https://doi.org/10.1256/smsqj.55706>
- Wood, C. R., Lacser, a., Barlow, J. F., Padhra, a., Belcher, S. E., Nemitz, E., ... Grimmond, C. S. B. (2010). Turbulent Flow at 190 m Height Above London During 2006–2008: A Climatology and the Applicability of Similarity Theory. *Boundary-Layer Meteorology*, *137*(1), 77–96. <https://doi.org/10.1007/s10546-010-9516-x>
- Wyngaard, J. C. (2004). Toward Numerical Modeling in the “Terra Incognita.” *Journal of the Atmospheric Sciences*, *61*(14), 1816–1826. [https://doi.org/10.1175/1520-0469\(2004\)061<1816:TNMITT>2.0.CO;2](https://doi.org/10.1175/1520-0469(2004)061<1816:TNMITT>2.0.CO;2)

## Figure Captions

Figure 1. Map of urban fraction used in the U100. The whole area shown is the 80 x 80 km domain used for U100 and U50. The smaller square shows the area of the 30 x 30 km domain of U100S. Also shown is the location of the observations – at this scale both the BT Tower and WCC are close to the tip of the arrow in the central area.

Figure 2 (a) 1.5m temperature field at 1400 UTC on the U100 domain. (b) Vertical velocity at 293m on the same domain.

Figure 3. Vertical velocity at 293m in (a) U100, (b) U50 and (c) U100S. In all cases the area shown is that of the domain of U100S. The North-South dotted line in (c) represents the location of the transect used in Figures 10 and 11 and the centre of the circle on the transect is the location of the BT tower (WCC close by on this scale). The scale to the right of (c) represents locations in km on the transect comparable to those on Figures 10 and 11.

Figure 4. Time/height cross sections of vertical velocity at WCC in (a) U100S (b) U100, (c) U50 and (d) lidar observations.

Figure 5. Profiles of sensible heat flux in U100 (left) U50. Dotted lines are parameterised flux, solid is explicit and dashed is total.

Figure 6. (a) Vertical velocity variance profiles from 1300-1400 UTC. Solid line is lidar data, dashed is U100 and dotted is U50 (b) theta profile in U100 and U50 averaged over a 2km box centred on the BT tower.

Figure 7. Mixing height at WCC as a function of time from lidar observations, U100 and U50. The mixing height was calculated using a variance threshold of  $0.1 \text{ m}^2\text{s}^{-2}$ . The solid line is lidar data, circles/dotted U100 and plus signs/dashes U50. Error bars were calculated by perturbing the variance threshold up and down by 30%.

Figure 8. Spectra for U100 and U50 compared to lidar and BT tower observations. Plus signs/solid lines BT tower, triangles/dashed lines lidar, diamonds/dash-dot U50 and squares/dotted lines U100.

Figure 9. Turbulence lengthscale as a function of height, both normalised by mixing height. Solid line is lidar data, dotted line from U50, dashed line from U100 and dash-dot line from Caughey et al., 1979.

Figure 10. Cross section of vertical velocity field (shading) and potential temperature (theta) contours in U100 at 1400 UTC along south (left) to north transect through BT tower with orography also shown.

Figure 11. South to north transect through BT tower showing urban fraction (dotted line) and plots for U100 (solid line) and U100S (dashed line). (a) mixing heights, (b) obukhov length (absolute value), (c) stability parameter.

Figure 12. Aspect ratio of vertical velocity objects as a function of distance from the southern boundary of the domain for U100 and U100S (dashed line) 100m model. A vertical velocity threshold of  $2.0 \text{ ms}^{-1}$  was used on a vertical velocity field on model level 20 (290m above ground). The aspect ratio data was smoothed as a function of distance from the southern boundary using an averaging length of 3km.

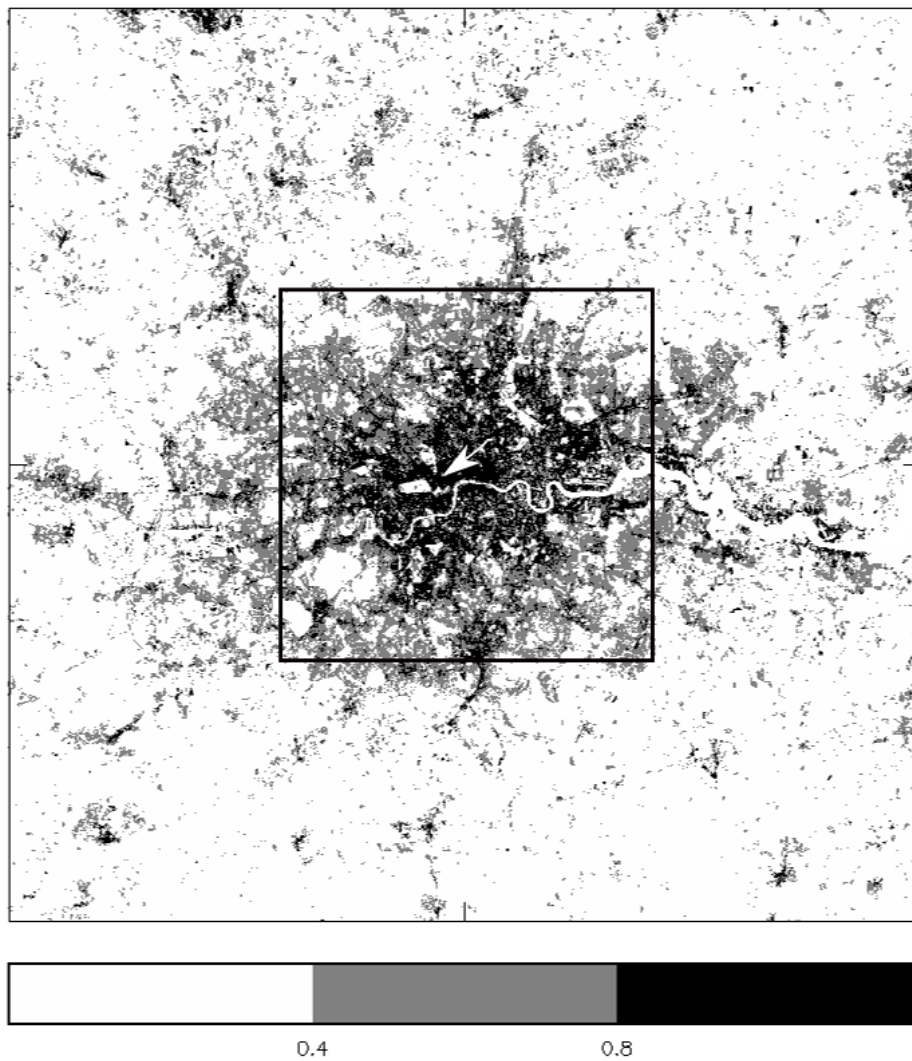


Figure 1. Map of urban fraction used in the U100. The whole area shown is the 80 x 80 km domain used for U100 and U50. The smaller square shows the area of the 30 x 30 km domain of U100S. Also shown is the location of the observations – at this scale both the BT Tower and WCC are close to the tip of the arrow in the central area.

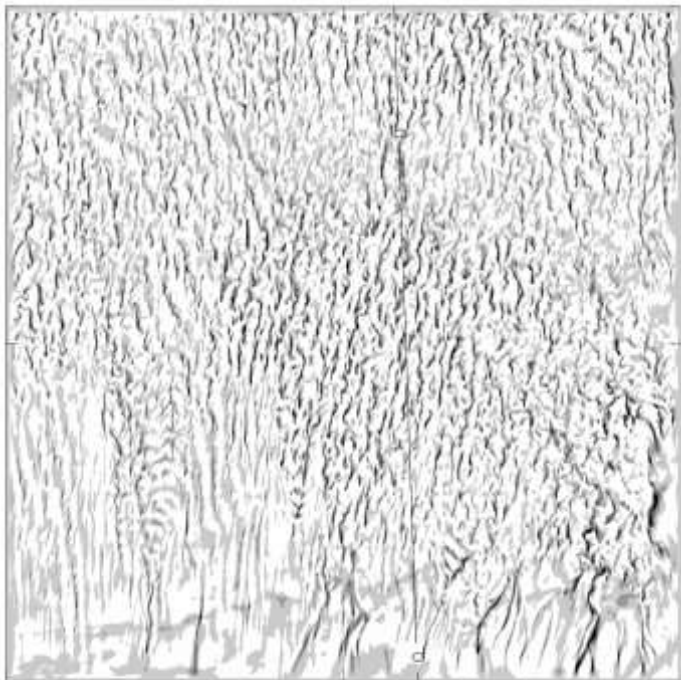
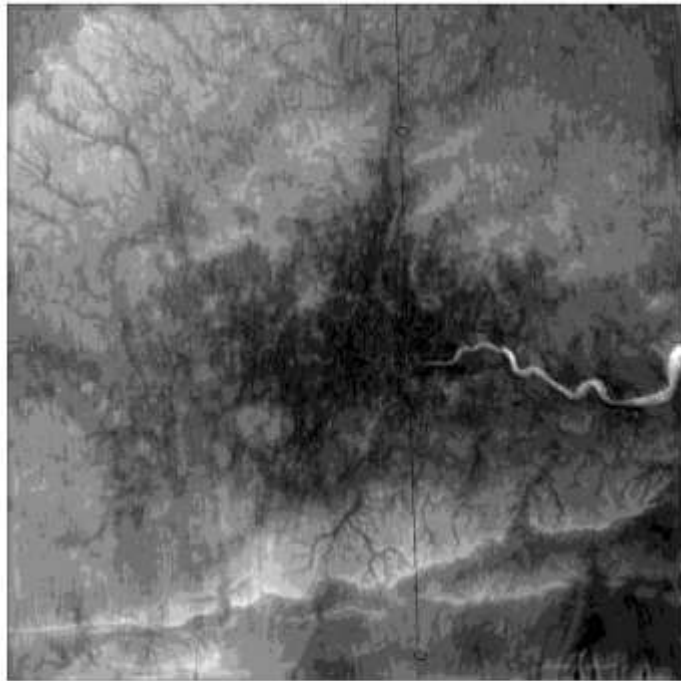


Figure 2 (a) 1.5m temperature field at 1400 UTC on the U100 domain. (b) Vertical velocity at 293m on the same domain.

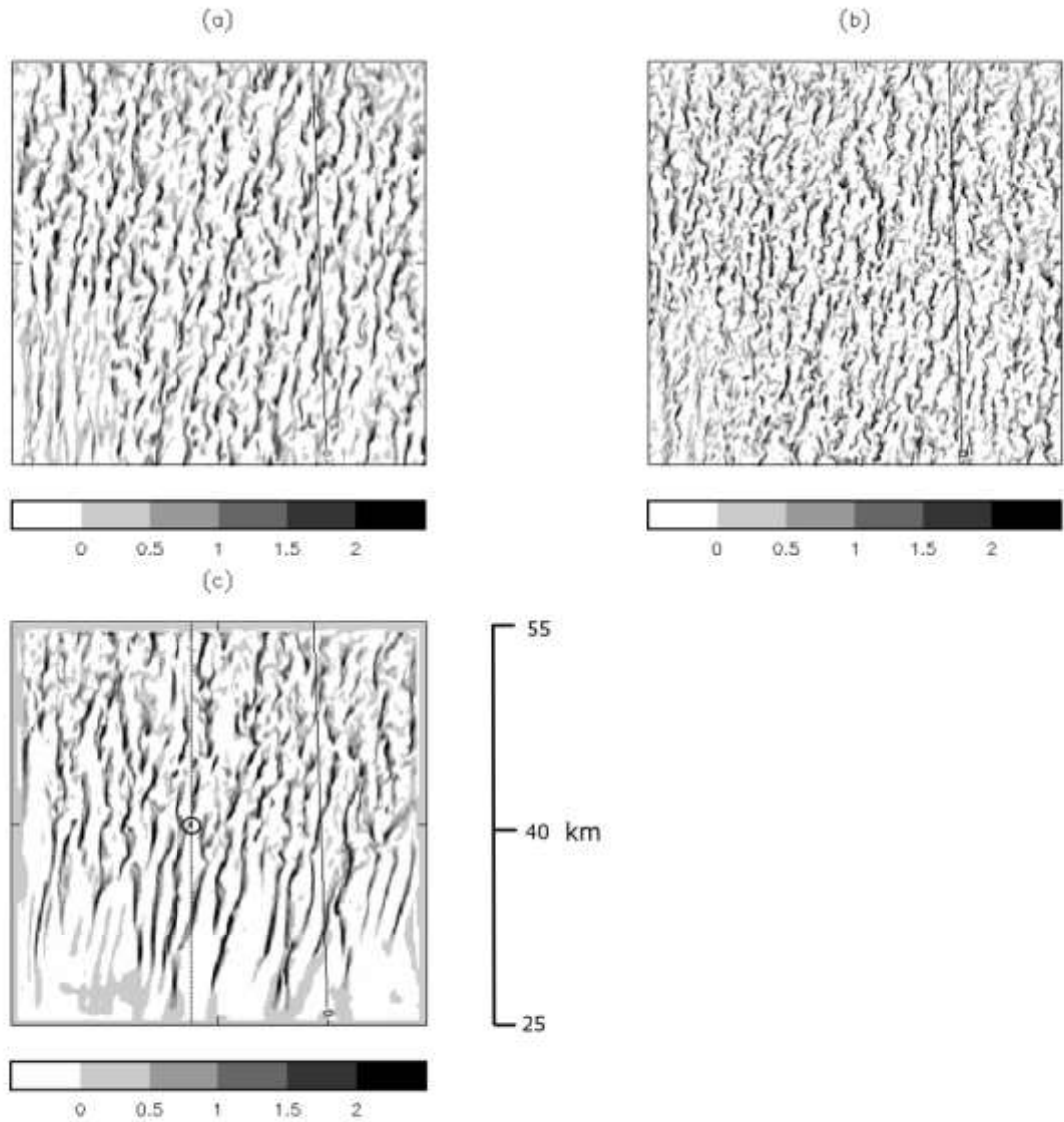


Figure 3. Vertical velocity at 293m in (a) U100, (b) U50 and (c) U100S. In all cases the area shown is that of the domain of U100S. The North-South dotted line in (c) represents the location of the transect used in Figures 10 and 11 and the centre of the circle on the transect is the location of the BT tower (WCC close by on this scale). The scale to the right of (c) represents locations in km on the transect comparable to those on Figures 10 and 11.

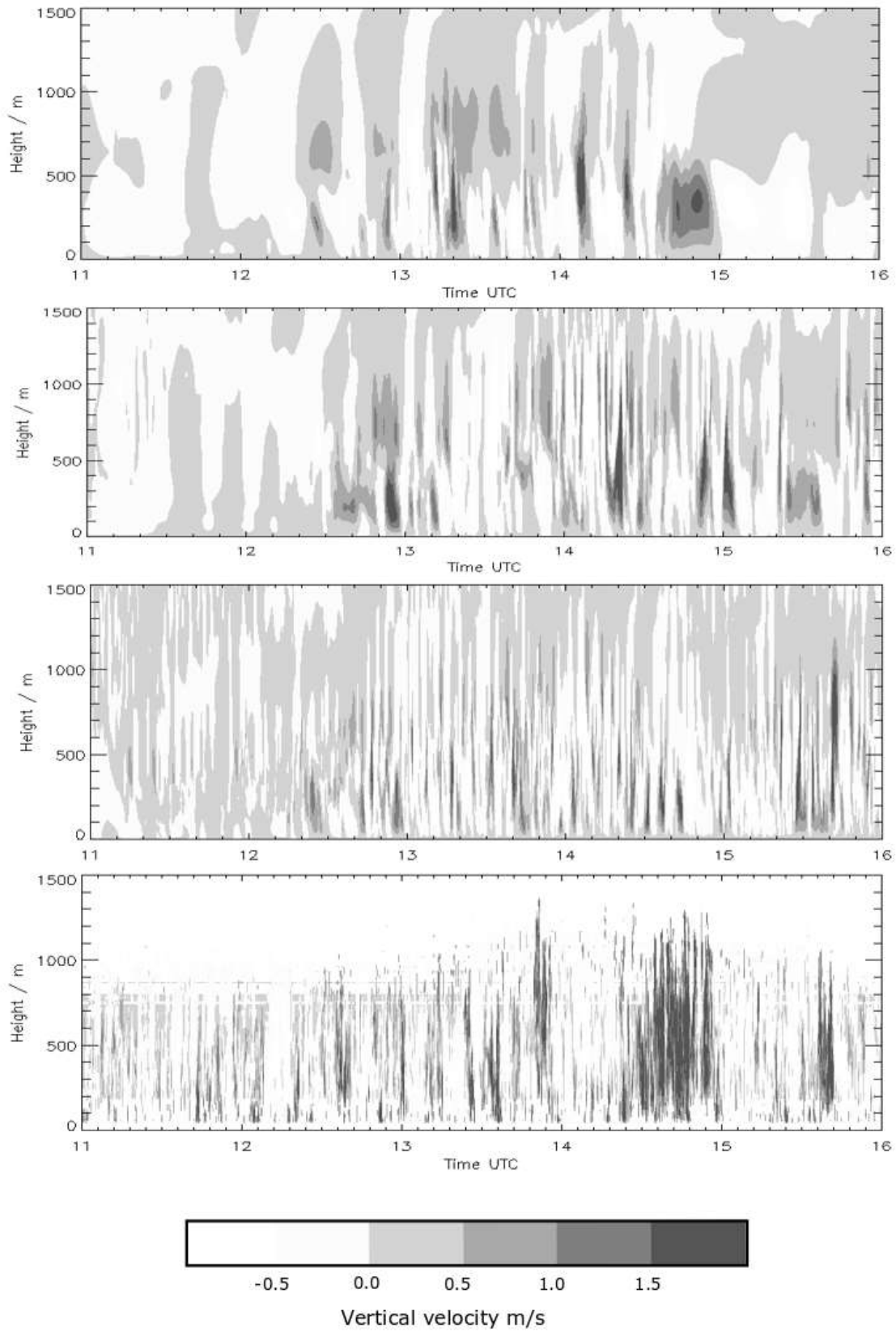


Figure 4. Time/height cross sections of vertical velocity at WCC in (a) U100S (b) U100, (c) U50 and (d) lidar observations.

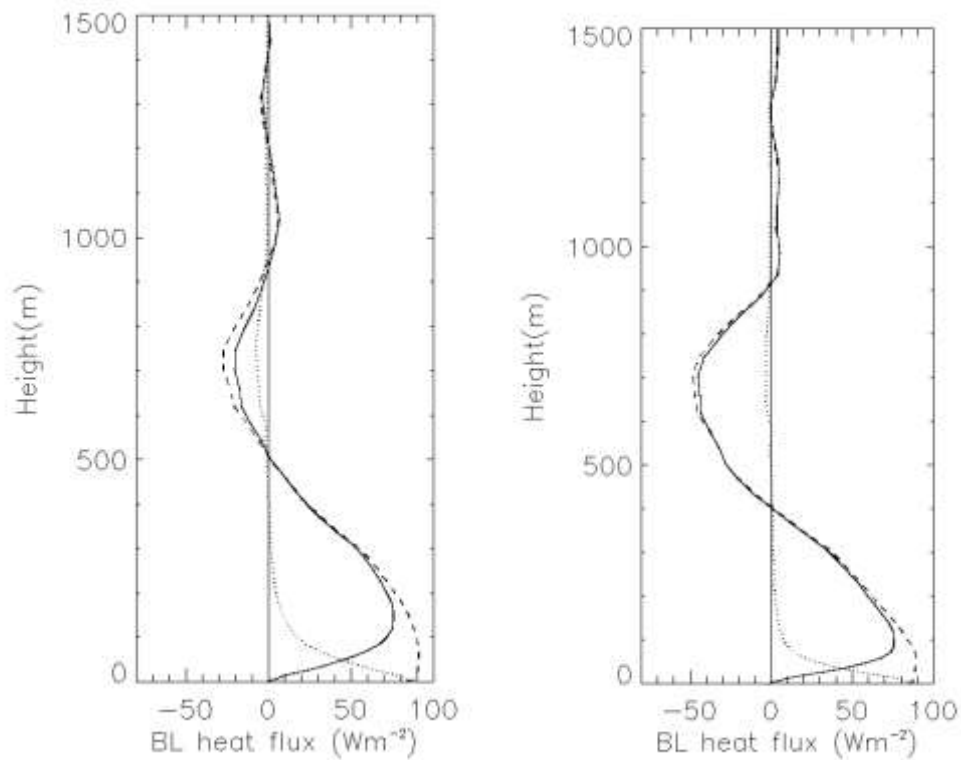


Figure 5. Profiles of sensible heat flux in U100 (left) U50. Dotted lines are parameterised flux, solid is explicit and dashed is total.

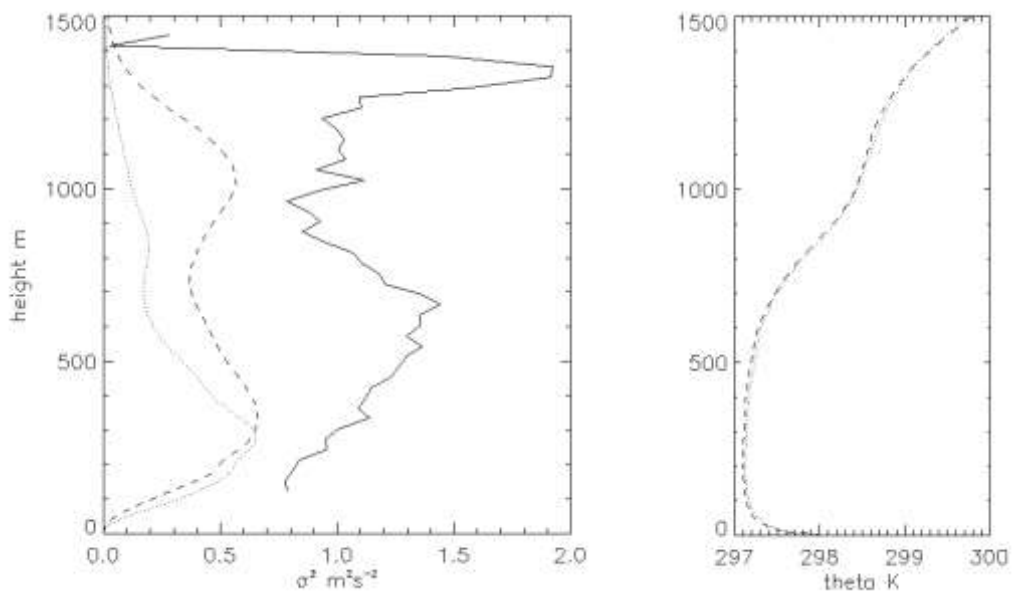


Figure 6. (a) Vertical velocity variance profiles from 1300-1400 UTC. Solid line is lidar data, dashed is U100 and dotted is U50 (b) theta profile in U100 and U50 averaged over a 2km box centred on the BT tower.

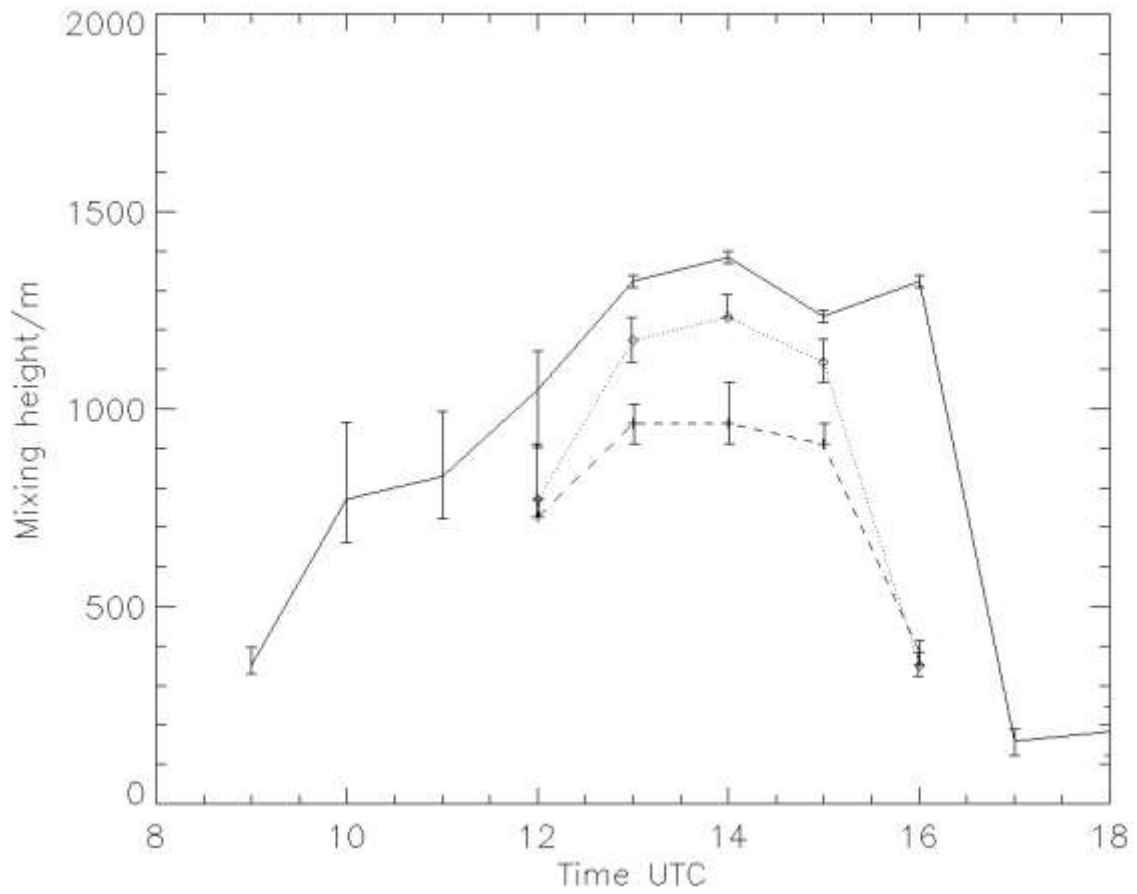


Figure 7. Mixing height at WCC as a function of time from lidar observations, U100 and U50. The mixing height was calculated using a variance threshold of  $0.1 \text{ m}^2\text{s}^{-2}$ . The solid line is lidar data, circles/dotted U100 and plus signs/dashes U50. Error bars were calculated by perturbing the variance threshold up and down by 30%.

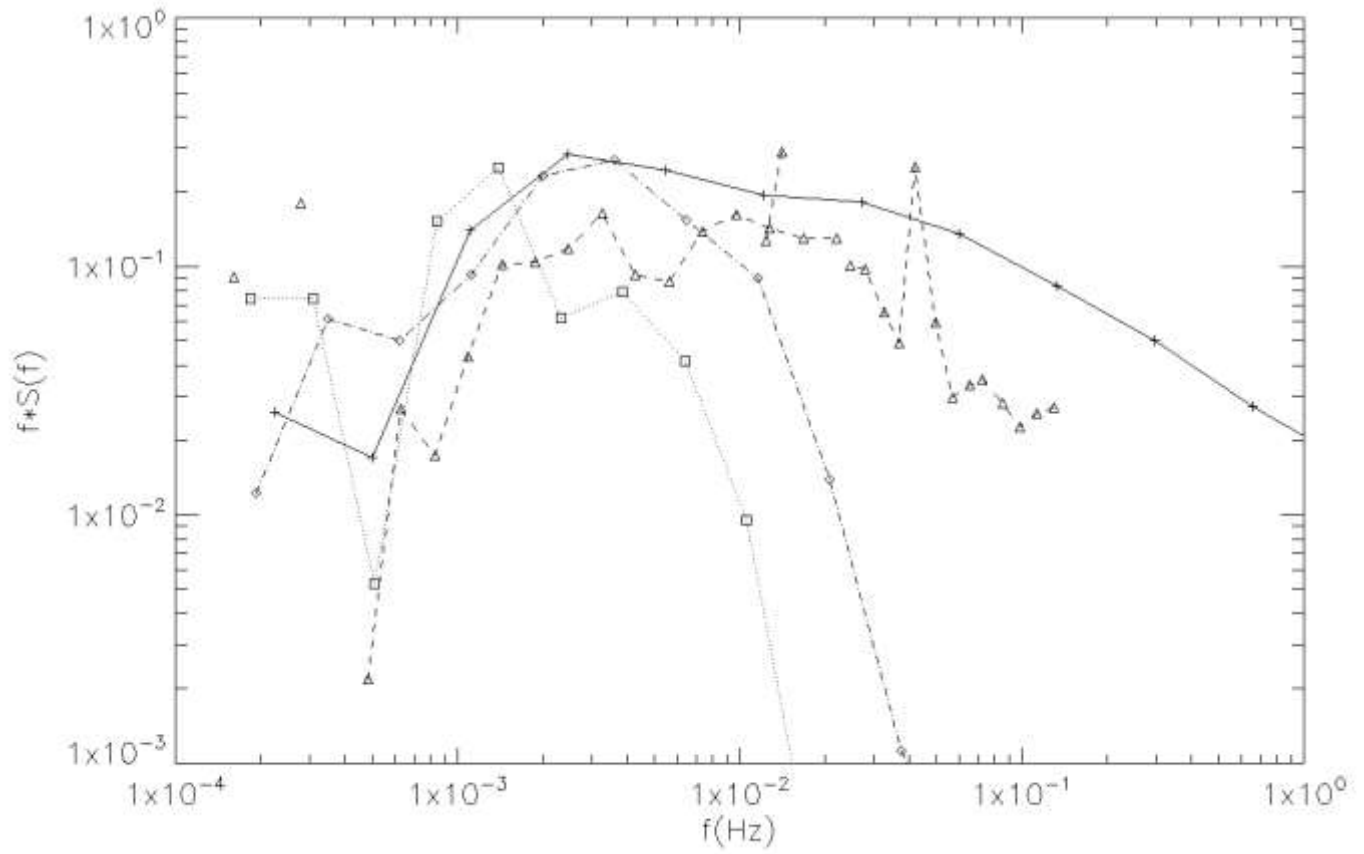


Figure 8. Spectra for U100 and U50 compared to lidar and BT tower observations for 1400 to 1600 UTC. Plus signs/solid lines BT tower, triangles/dashed lines lidar, diamonds/dash-dot U50 and squares/dotted lines U100.

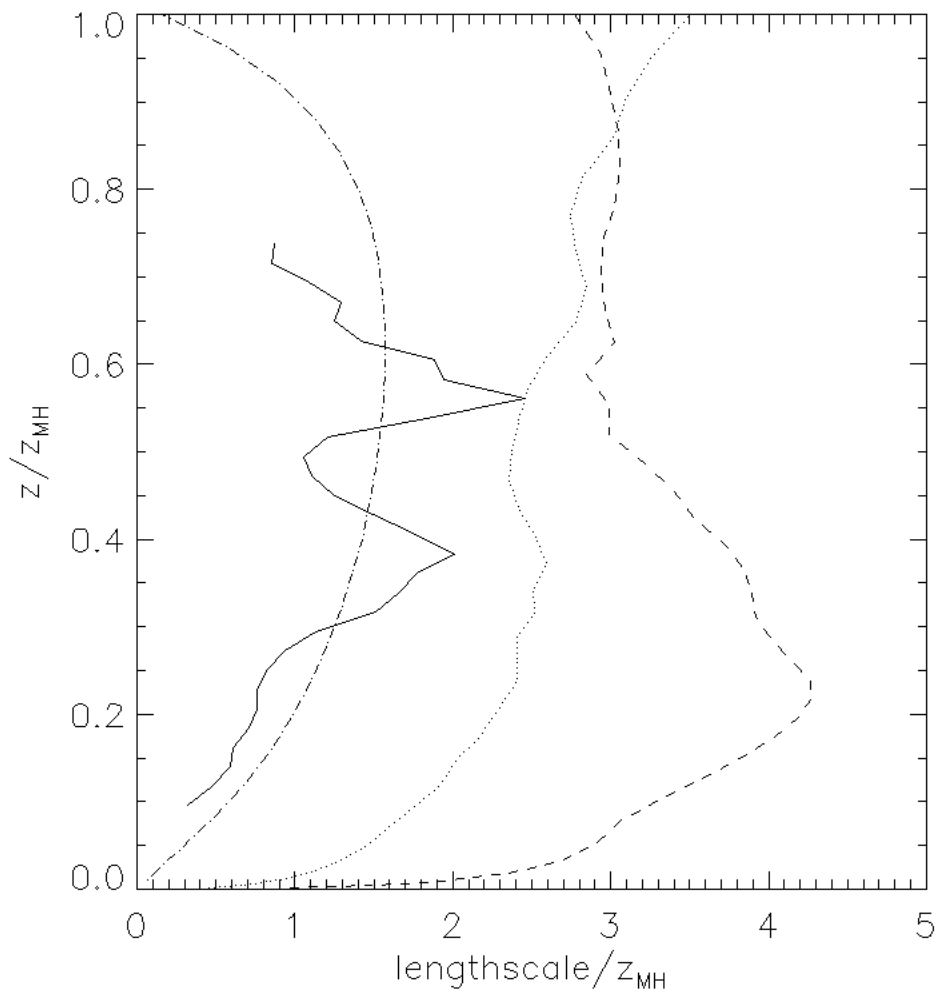


Figure 9. Turbulence lengthscale as a function of height for 1400 to 1600 UTC, normalised by mixing height. Solid line is lidar data, dotted line from U50, dashed line from U100 and dash-dot line from Caughey et al., 1979.

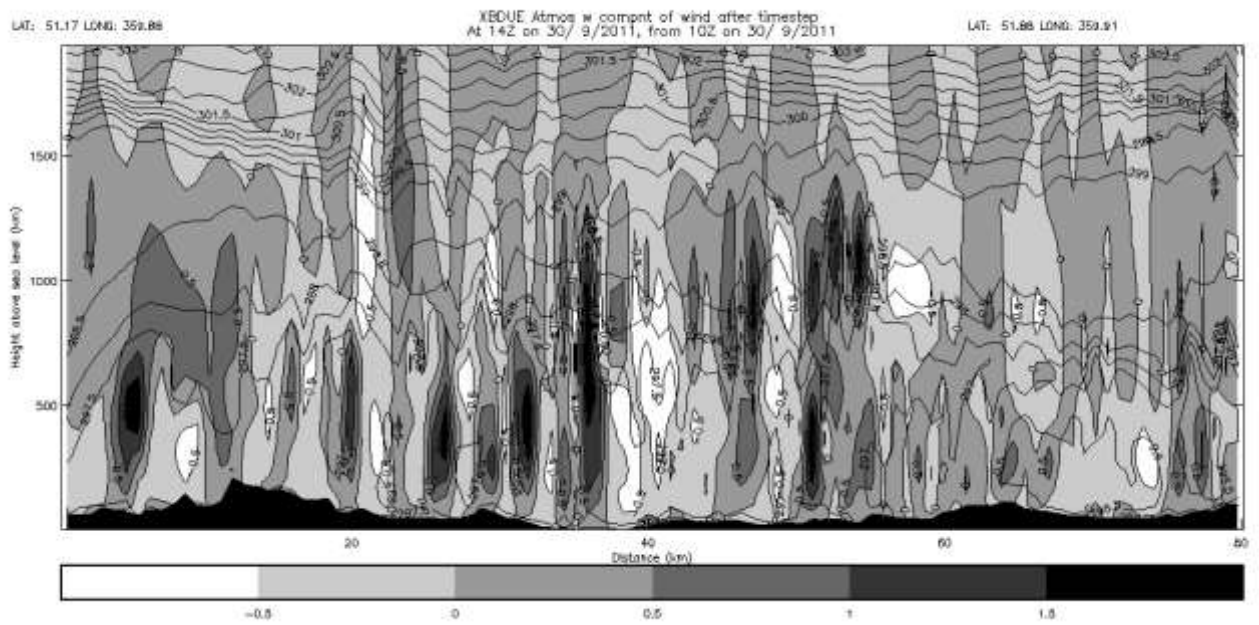


Figure 10. Cross section of vertical velocity field (shading) and potential temperature ( $\theta$ ) contours in U100 at 1400 UTC along south (left) to north transect through BT tower with orography also shown.

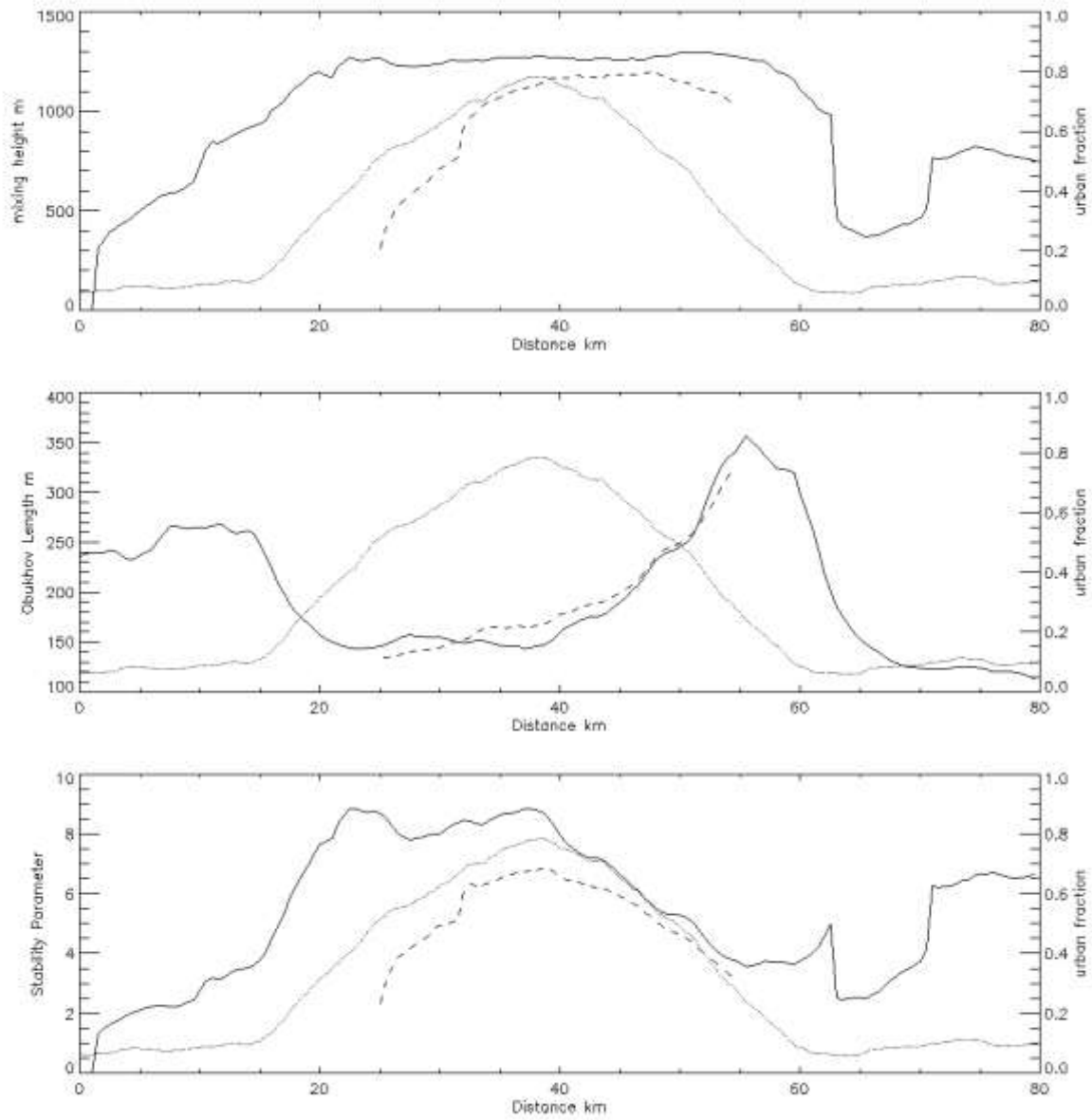


Figure 11. South to north transect through BT tower showing urban fraction (dotted line) and plots for U100 (solid line) and U100S (dashed line). (a) mixing heights, (b) obukhov length (absolute value), (c) stability parameter.

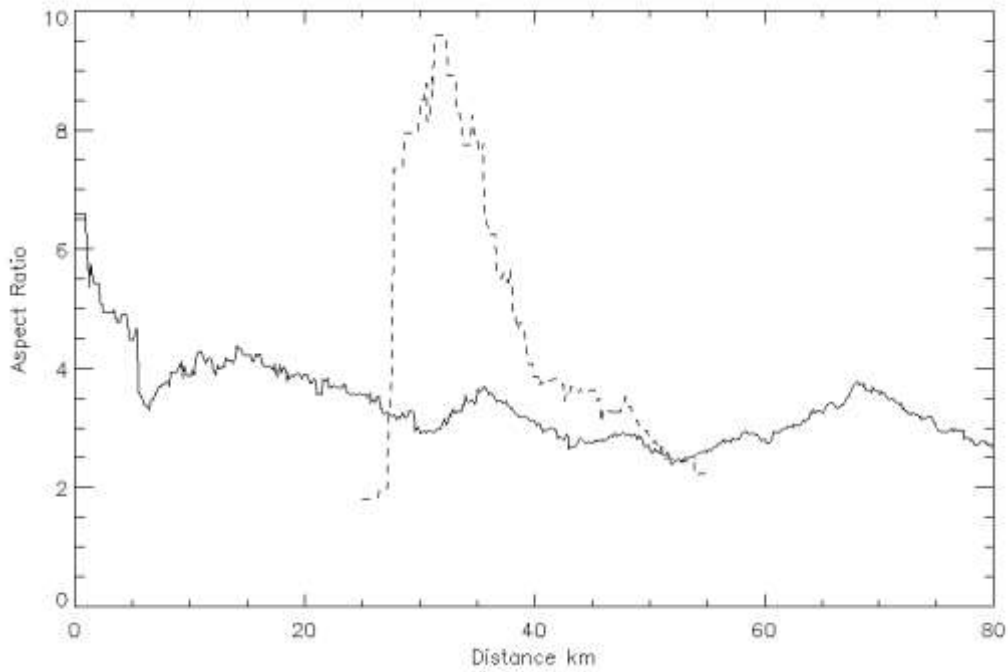


Figure 12. Aspect ratio of vertical velocity objects as a function of distance from the southern boundary of the domain for U100 and U100S (dashed line) 100m model. A vertical velocity threshold of  $2.0 \text{ ms}^{-1}$  was used on a vertical velocity field on model level 20 (290m above ground). The aspect ratio data was smoothed as a function of distance from the southern boundary using an averaging length of 3km.